Supporting Information

for

Room Temperature MIR Detection through Localized Surface Vibrational States of SnTe Nanocrystals

Matthew E. Cryer and Jonathan E. Halpert[§,]*

MacDiarmid Institute for Advanced Materials and Nanotechnology, School of Chemical and Physical Sciences, Victoria University of Wellington, P.O. Box 600, Wellington, New Zealand.

J.E. Halpert ORCID ID: 0000-0002-9499-2658

E-mail: jonathan.halpert@vuw.ac.nz; jhalpert@ust.hk

*corresponding author(s): J.E.H.

§ see Author Information for present address

SA. XRD
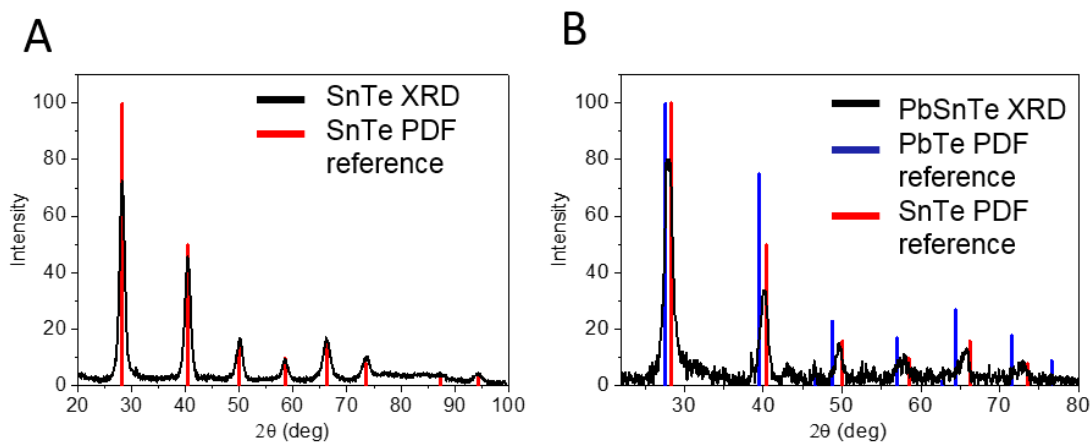
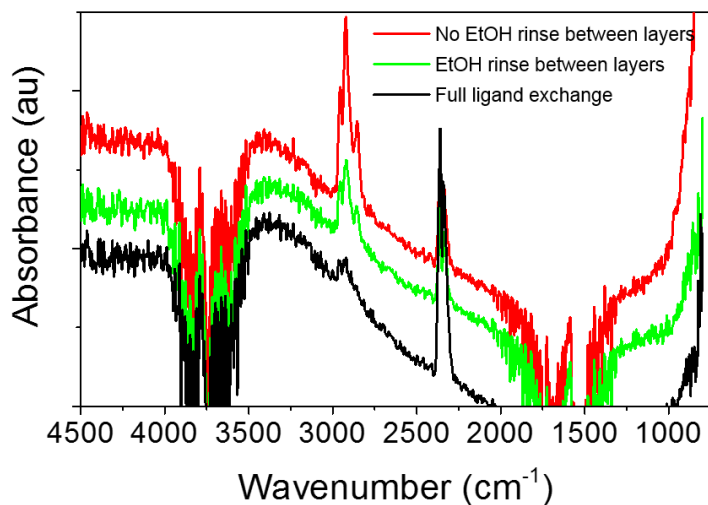**Figure S1**. XRD data and reference for dried films of the A, 12 nm SnTe and B, PbSnTe QDs, the PbSnTe peaks sit between the reference spectra of SnTe and PbTe. There are no peaks attributable to oxides in the XRD data. Indicating that the majority of each QD is pure semiconductor lattice.

SB. Ligand exchange
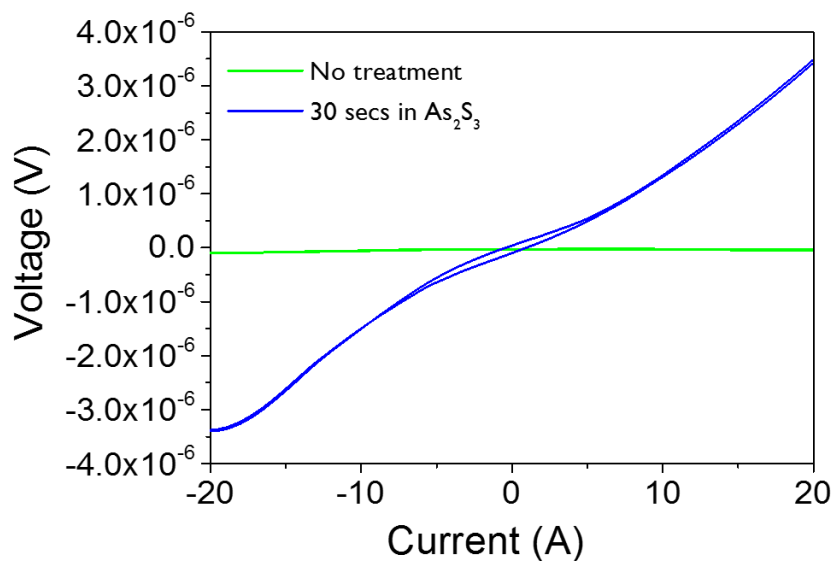
Figure S2. IV curve of device before and after the ligand exchange.

Figure S3. Film absorbance of SnTe films (identical in all other respects) made with different processes, vertically separated for clarity. If the film is rinsed with ethanol but no ligand exchange is conducted then there is still a reduction in organics, but not as severe as with the

ligand exchange. This suggests that the exchange is actually removing the oleic acid, not just removing excess organics from the film.

SC. TEM of QDs
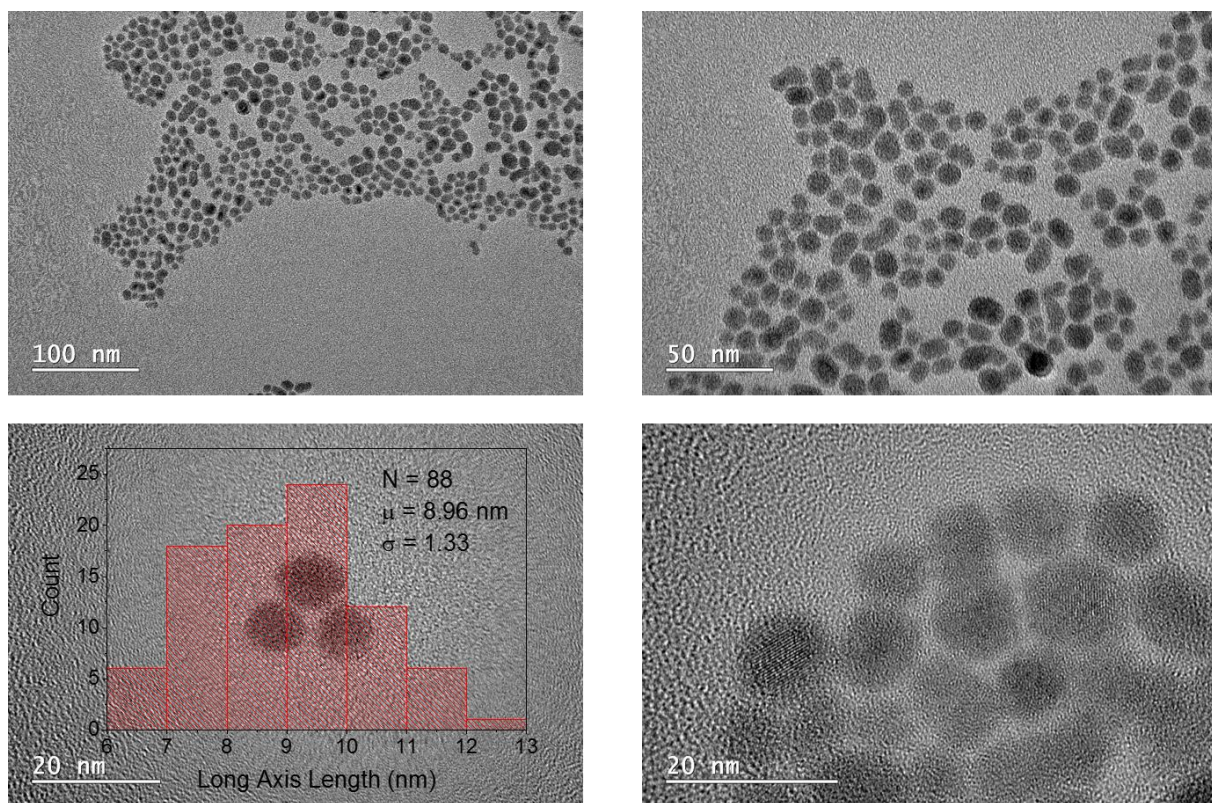
Figure S4. TEM images and sizing of the 8.9 nm SnTe QDs.
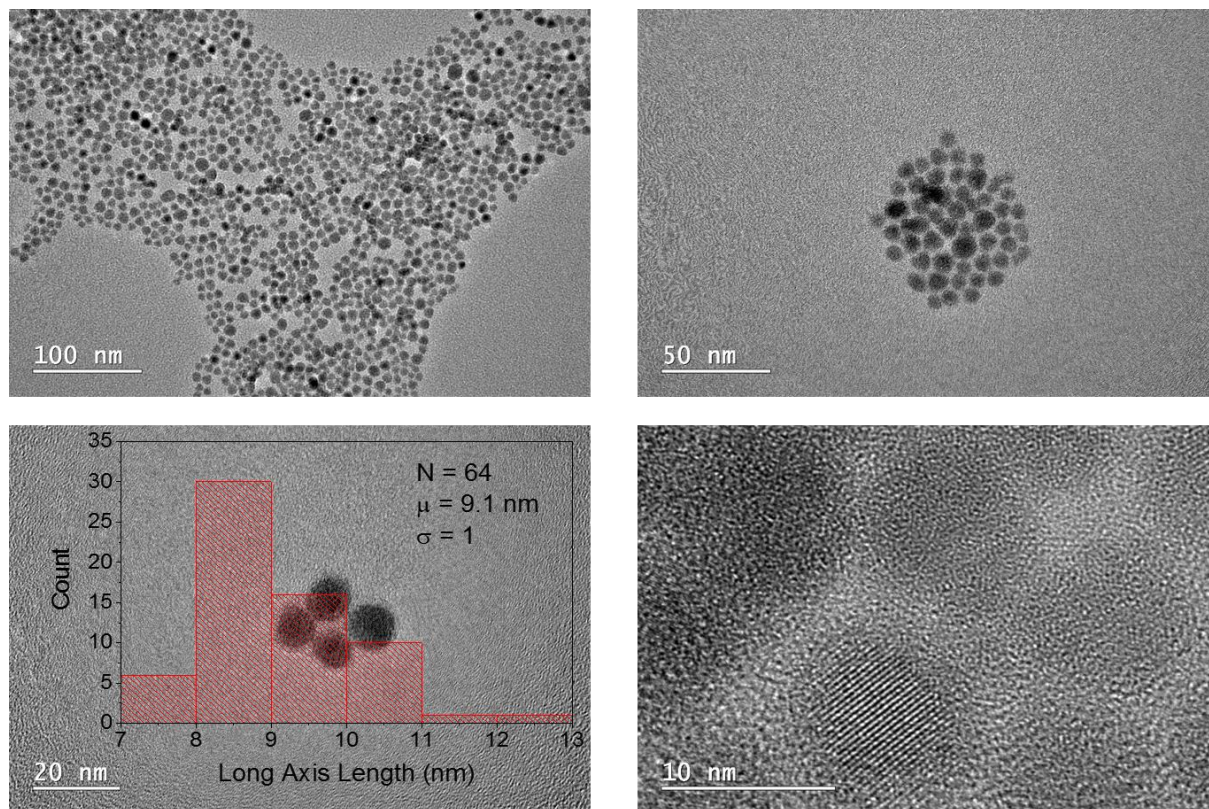
Figure S5. TEM images and sizing of the 9.1 nm SnTe QDs.

Figure S6. TEM images and sizing of the 11.4 nm SnTe QDs.
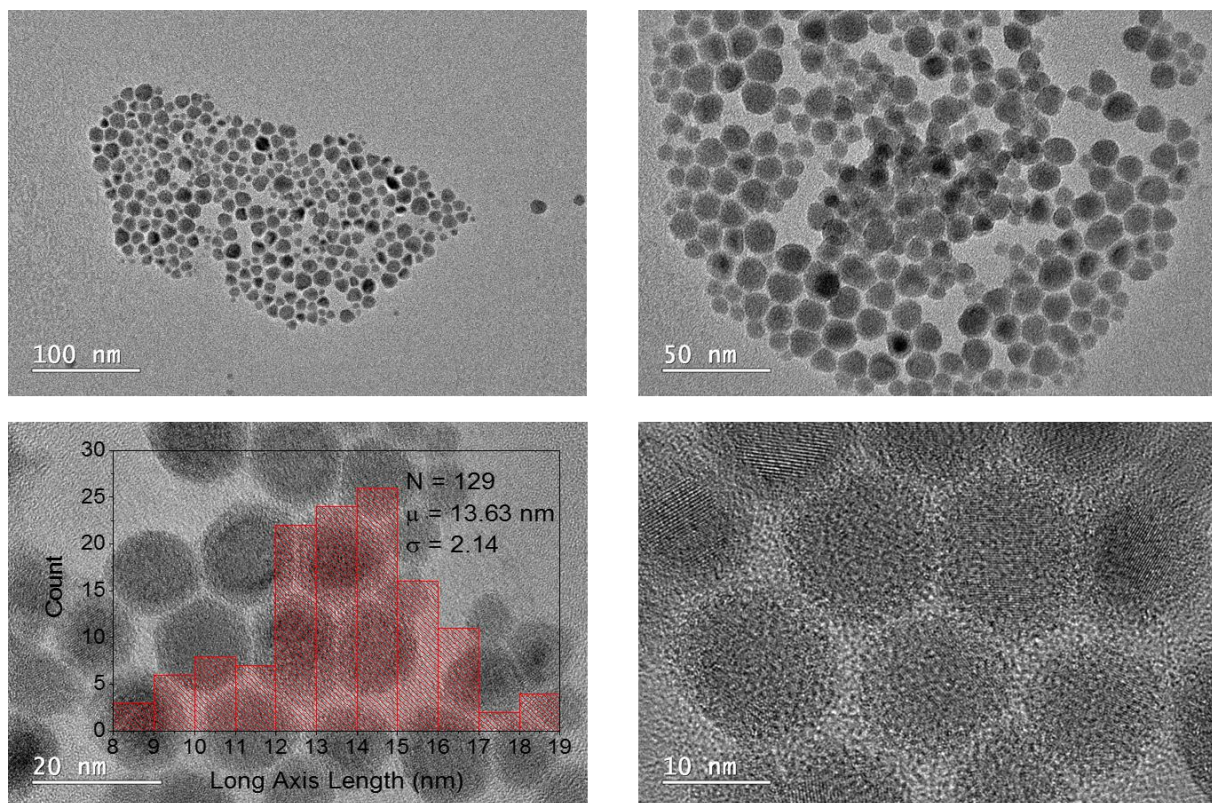
Figure S7. TEM images and sizing of the 13.6 nm SnTe QDs.
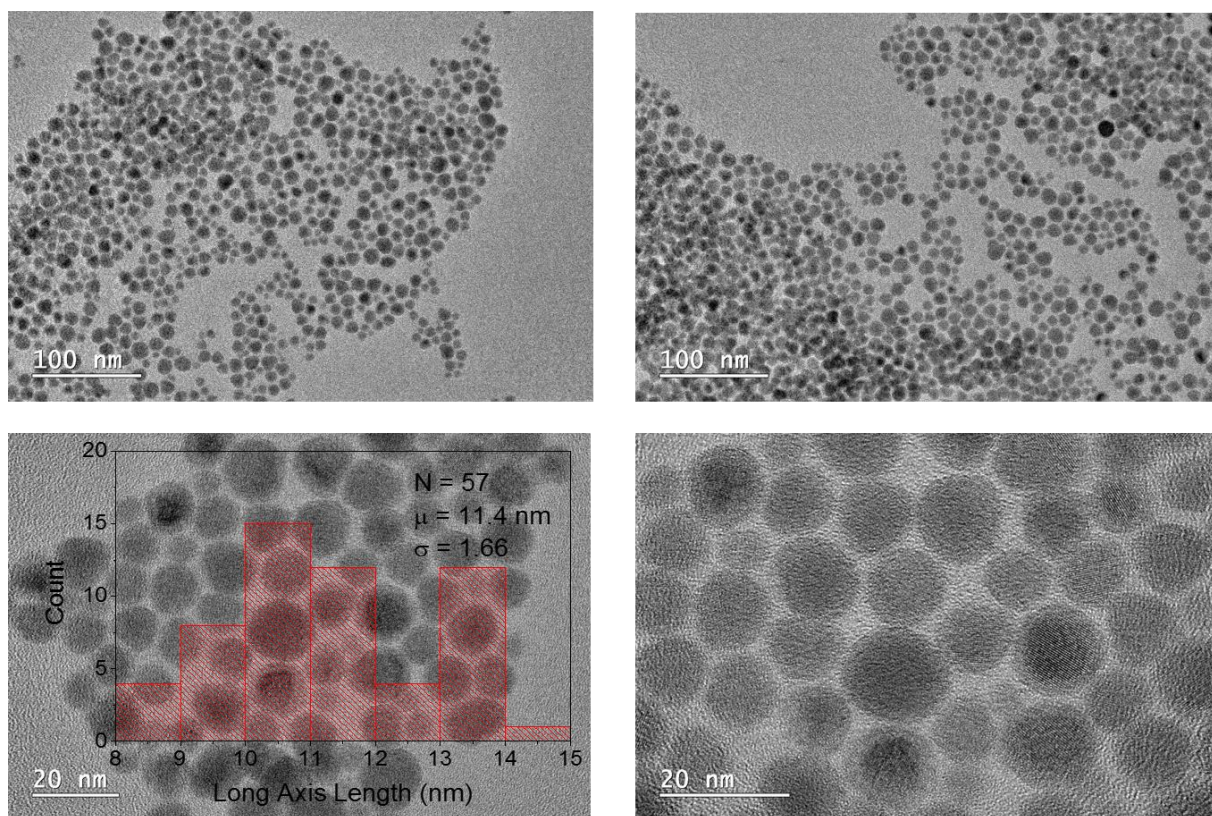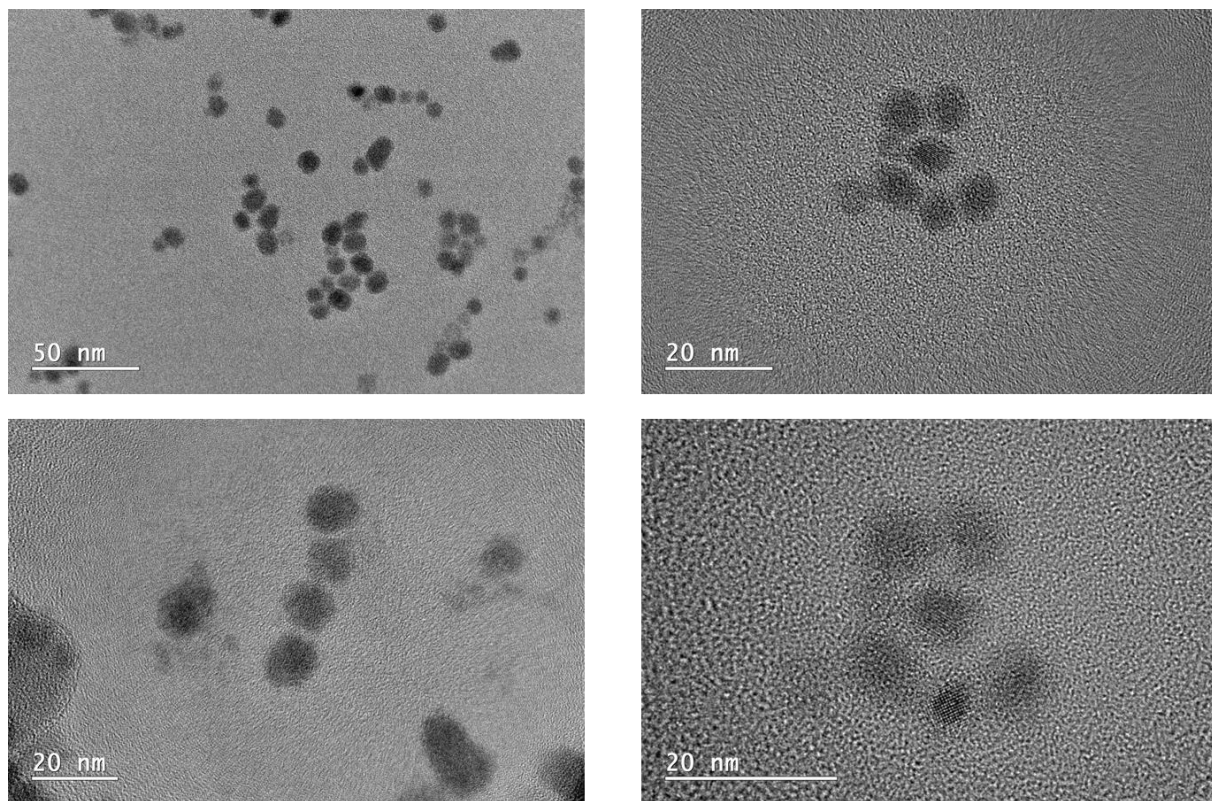
Figure S8. TEM images and sizing of the PbSnTe QDs from the preparation that most closely matched the idealized composition of $Pb_{0.3}Sn_{0.7}Te$.[1] Only QDs that showed this composition, as measured by XRD peak position and lattice fringe spacing were used in devices that are shown in this paper due to the previously published work on this materials identifying this as the optimal composition.
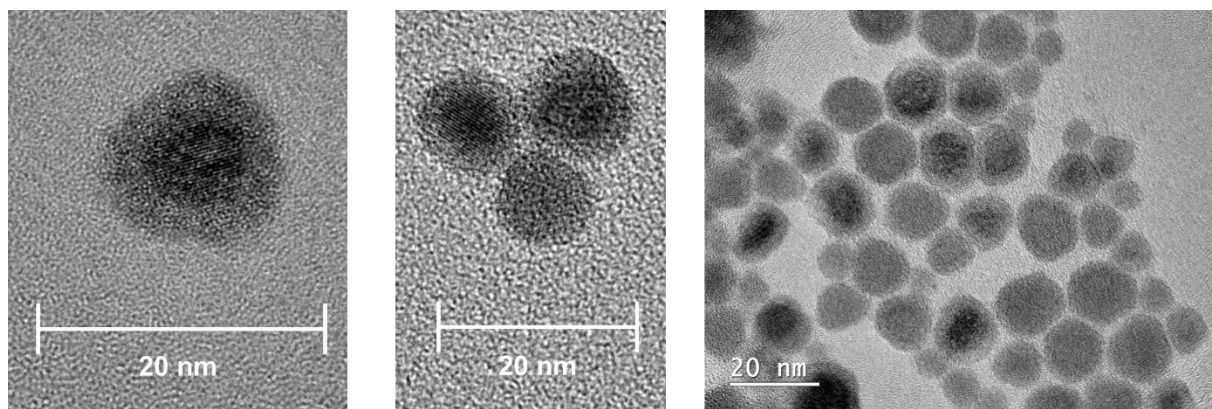
Figure S9. TEM images of various QDs showing a visible amorphous shell.

SD. STEM Mapping
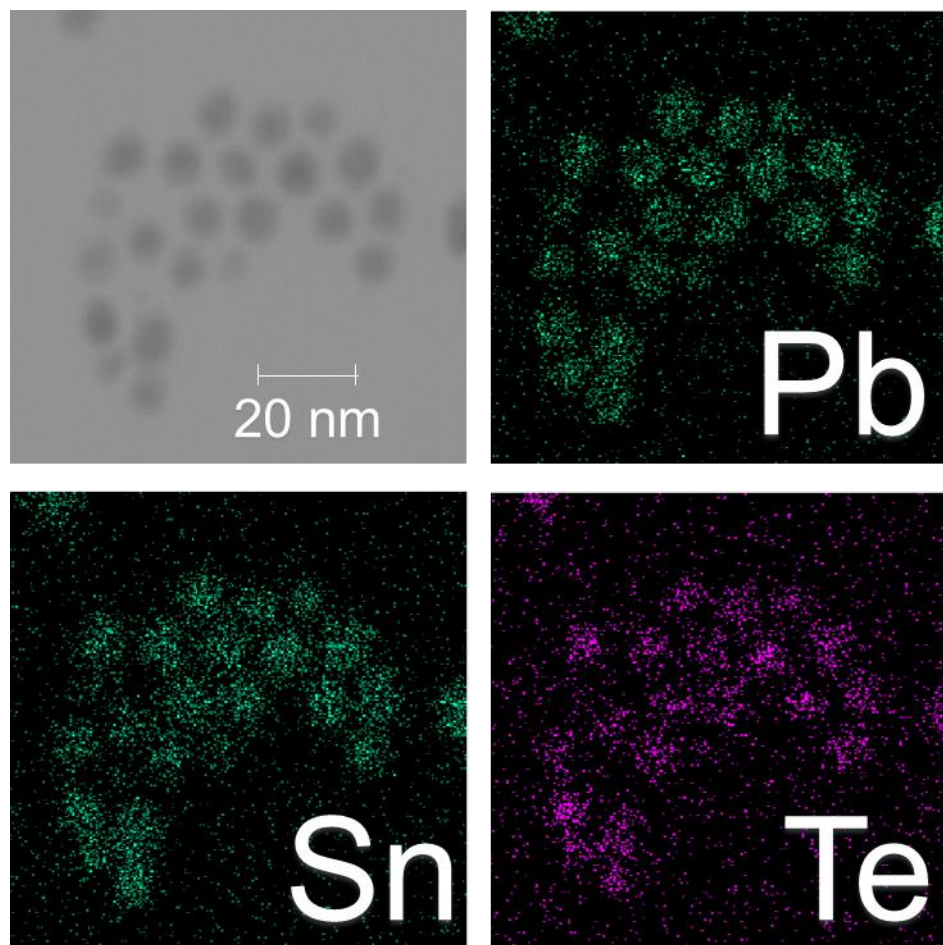
Figure S10. STEM mapping of PbSnTe NCs.
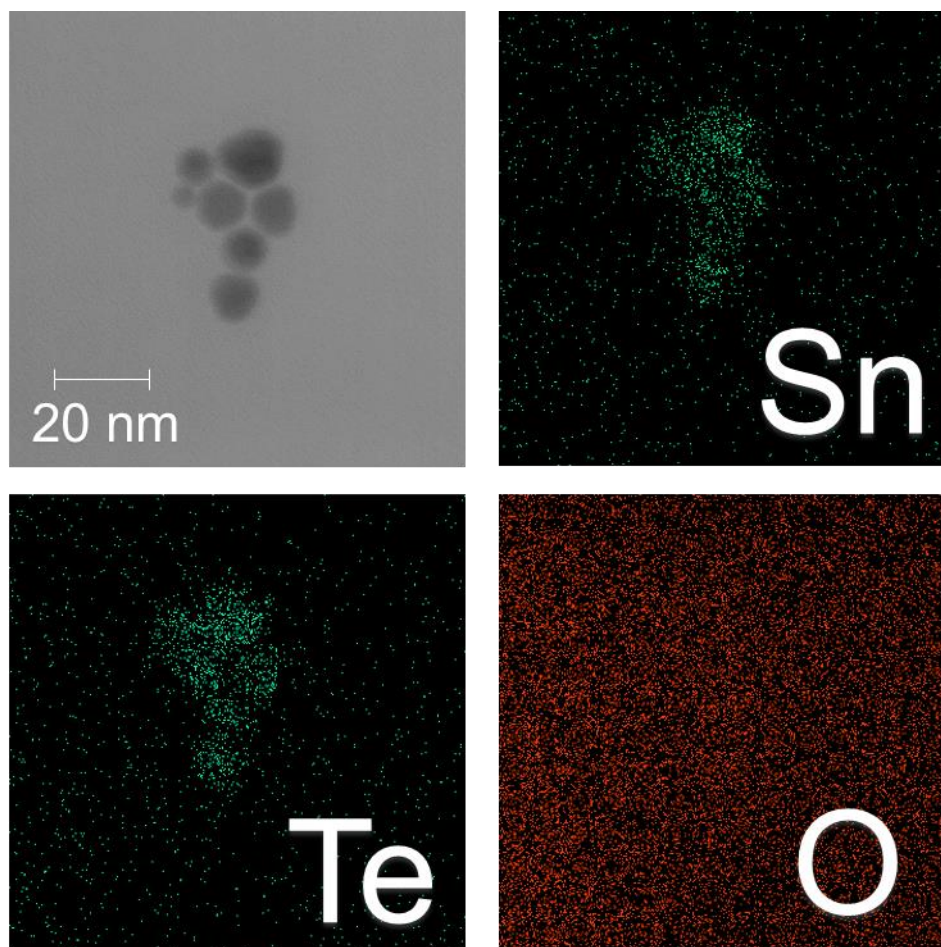
Figure S11. STEM mapping of SnTe NCs.

SE. SEM EDS Mapping
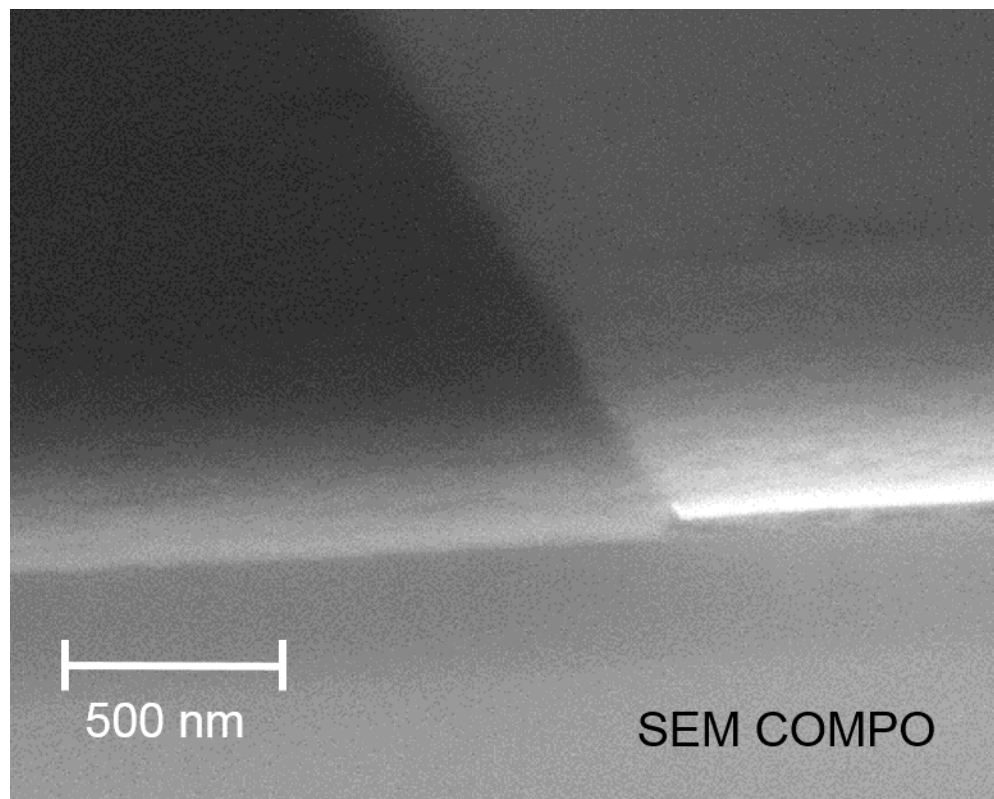
Figure S12. SEM composite image of SnTe device.
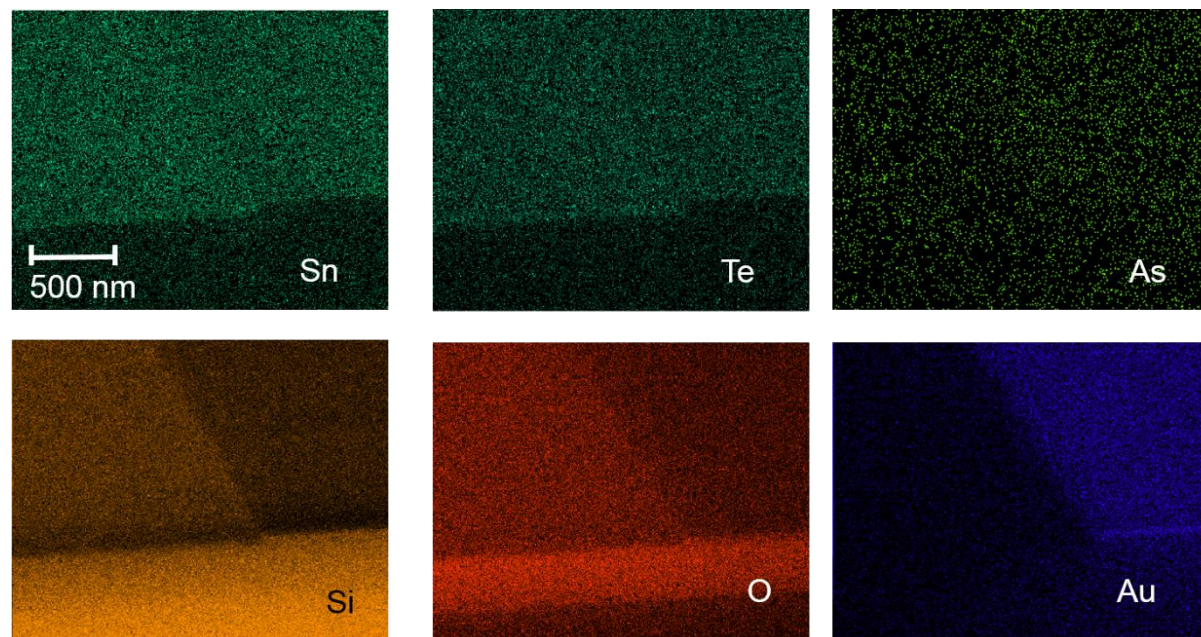
Figure S13. SEM STEM EDS mapping of the same area of device as shown above and in Figure 1D.

Machine	QDs used on device	Mean ratio by atomic %	
		Sn	Te
JEOL 6500F	8.9 nm SnTe	1.44	1
JEOL 6500F	8.9 nm SnTe	1.26	1
JEOL 6610LA	13.6 nm SnTe	1.76	1
JEOL 6610LA	13.6 nm SnTe	1.69	1
JEOL 6610LA	13.6 nm SnTe	1.71	1

Table S1. Composition ratio of different locations on the surface of two devices as measured by EDS in two separate SEMs.

SF. TEM EDS and ICP-MS

Sample	TEM EDS Atomic Ratio		ICP-MS Atomic Ratio		Notes
	Sn:Te	Pb:Te	Sn:Te	Pb:Te	
SNR1	1.06	N/A	0.84	N/A	5 ml OLA / 15 ml ODE
SNR2	1.78	N/A	1.53	N/A	7.5 ml OLA / 12.5 ml ODE
SNR3	1.76	N/A	1.56	N/A	10 ml OLA / 10 ml ODE
PNR1	2.83	3.25	2.73	3.19	Prep used as in section SI/SJ

Table S2. TEM EDS and ICP-MS data for 6 samples.

Both methods are reasonably accurate, however there is consistent discrepancy with the ICP-MS data giving higher Te values (lower ratios) than the TEM EDS (and SEM EDS Table S1). ICP-MS samples were run for a large number of samples and this difference remained. It is attributed to the oxygen displaced Te remaining in the samples run through the ICP-MS. Comparatively, the TEM EDS samples were targeted on areas of high QD density so would not include remaining Te precursor in the same ratio. In all cases the dearth of tellurium is a good indication of tin oxide forming at the surface of the QD after processing, as can be seen in the TEM images.

SG. Time Response of Device
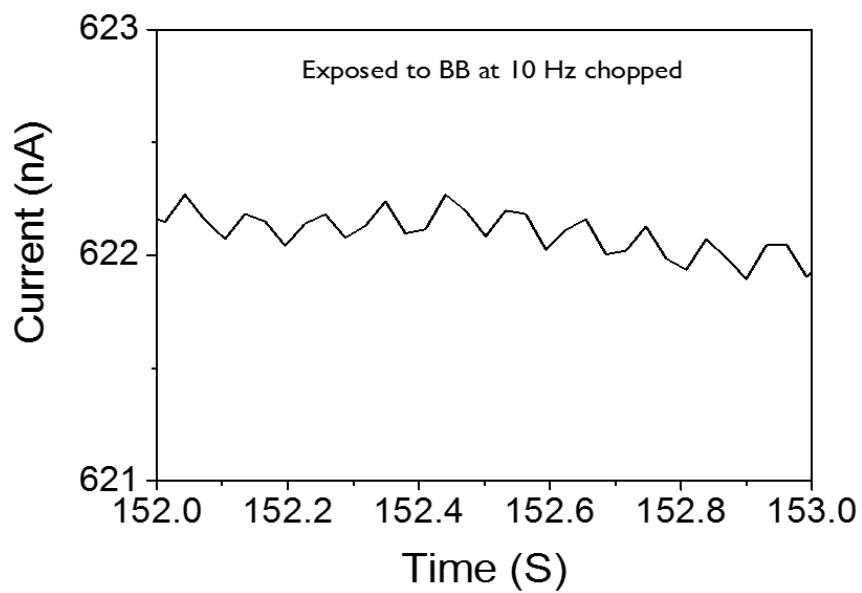
Figure S14. Current vs time plot when the 3 – 6 µm signal from a 1073 K blackbody is chopped at 10 Hz in the PbSnTe device.

SH. STEM EDS of Te NW / QD blend
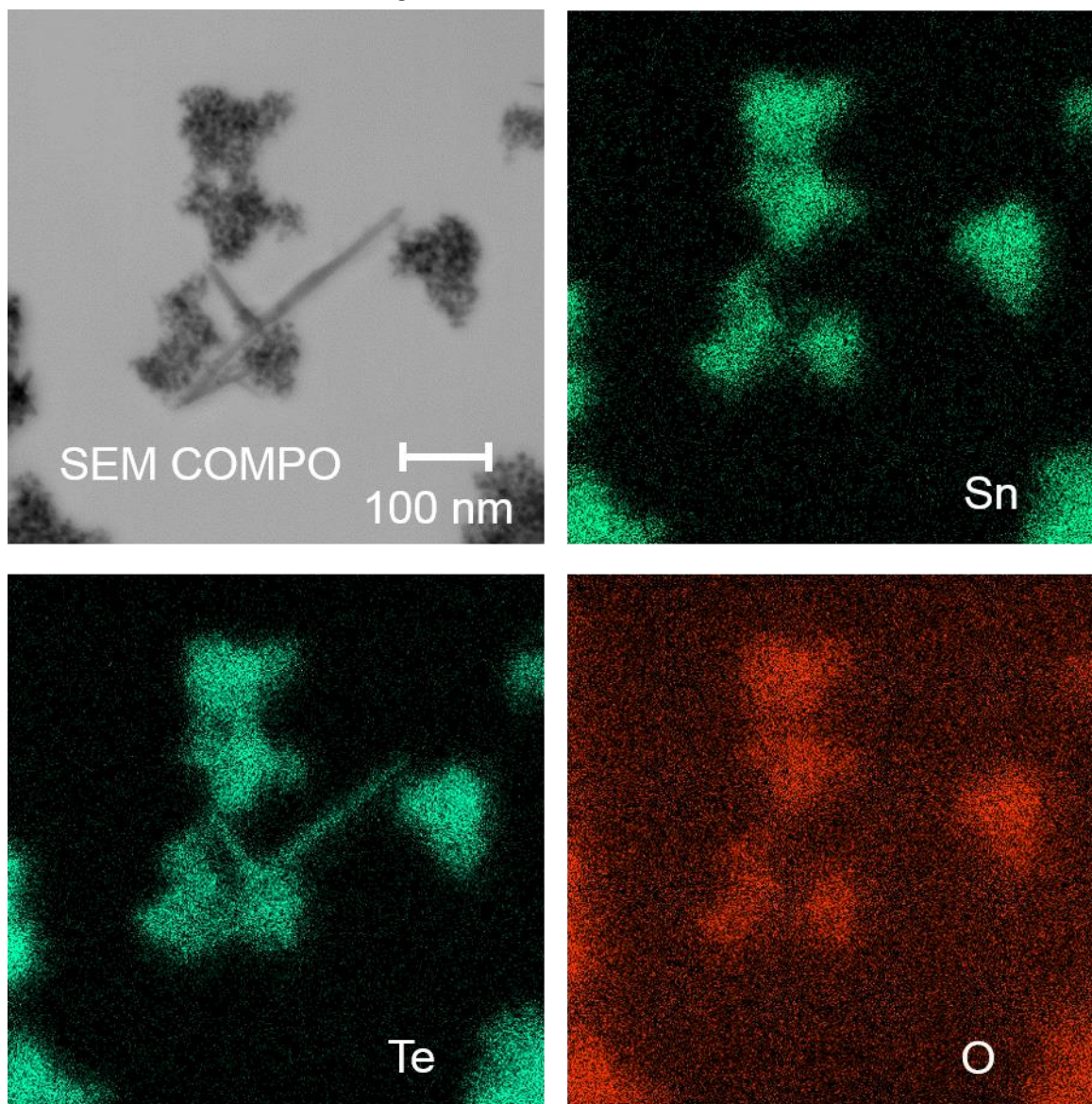
Figure S15. STEM EDS mapping of a prep with a sufficiently low oleylamine content to allow the formation of Te NWs. It can be seen that the NW features do not show any oxygen signal, whereas the QD clusters do show an oxygen signal above the background. It is clear that within the same colloidal suspension the Sn surfaces have adsorbed oxygen and the purely Te surfaces have not. This strongly suggests that the Sn is the oxygen bonding site. There is no lead in this sample.

SI. Synthesis details and full experimental method

PbSnTe QDs were synthesized using a two-step hot injection method. In a typical synthesis 56 mg of $PbCl_2$ was dissolved in 12.5 ml of oleylamine (OLA) and the mixture was then degassed under vacuum at 120 °C for 1 hour. The mixture was then placed under nitrogen and 0.16 ml of bis[bis(trimethylsilyl)amino]tin(II) in 7.5 ml of dry octadecene (ODE) was injected and the temperature raised to 150 °C, 0.73 ml of a dry 1 M trioctylphosphine: tellurium (TOP:Te) precursor was then injected and the mixture instantly turned black. The heat was removed, the mixture was left for 90 s and then quenched by submerging the vessel in ice water, followed by the injection of 3 ml of oleic acid (OA). Once at 25 °C, 10 ml of 1:1 chloroform: acetone is added and the mixture can then be either stored or processed. QD purification was performed in air by centrifuging with acetone / chloroform as the anti-solvent / solvent pair.

PbTe QDs were synthesized using the same method without the Sn precursor. For PbTe the mixture does not turn black until 180 °C and was heated at this temperature for 20 mins before quenching.

SnTe QDs were synthesized using the same method without the Pb precursor. Differing sizes were achieved by varying the OLA concentration in the mixture. Exact details can be found in Table S3.

TEM samples were placed on Agar 300 mesh Cu on Formvar grids, colloids were washed 4 times and dispersed in tetrachloroethylene before being placed on the grids. Before imaging the grids were oxygen plasma cleaned for 30 mins. TEM, STEM and EDS measurements were done on a JEOL-2100 TEM.

Absorbance measurements were done on a Bruker Tensor 27 FTIR with a diamond ATR attachment and a VISNIRMIR Bruker Vertex 80v. All film measurements were done on 1 mm

thick CaF_2 substrates purchased from Eskma Optics. QDs were spin coated onto substrates and devices at 1K rpm for 40 secs. In between layers the films were treated with a ligand exchange solution of 5 mg As_2S_3 in 30 ml propylamine and 30 ml ethanol and then rinsed in ethanol. Due to the low wetting angle of CaF_2 compared to silane treated SiO_2 the absorption of the CaF_2 films provides a low estimate of the absorption of the film on the SiO_2 devices.

Device substrates were Si/SiO_2 wafers with 300 nm oxide layers. The first step in fabrication was surface treatment ((3-aminopropyl)trimethoxysilane in dry toluene for 30 minutes) to deposit a silane self-assembled monolayer (SAM) and then Cr/Au (5/50 nm) inter-digitated electrodes (IDE) (36 fingers per side, 2 mm x 20 µm with 10 µm spacing, device area is 4×10^{-6} m^2) networks were 1-step photo-lithographically deposited. All devices had drain – source leakage currents below 10 pA and gate – source leakage below 1 nA before QD films were deposited.

Electrical measurements were completed on a Keithley SCS-4200 parameter analyzer with the device in ambient atmosphere in the sample chamber of an uncooled Janis VNF-100 optical cryostat. Both the mount and the chamber were monitored for temperature change during measurements. With optical filters in place the maximum recorded temperature change during measurement was 0.05 K / min. The optical path for device illumination consisted of the cavity opening of an Omega BB-4A blackbody, 12 cm of air shielded from external light, the long pass filter, the chopper blade and two sapphire windows. Incident flux was calculated using a spectrally integrated plank function over the transmittance of the path and the effective solid angle obtained from calibration using a Thorlabs PM-100D with S401C power meter. To remove any extant background effects the change in current was recorded for the BB being covered/exposed rather than the sample chamber being covered. Responsivity was calculated as the difference between the current during exposure and the current level to which the device

returned once the IR radiation was removed, in order to avoid errors arising from film degradation. To conclusively prove that some aspect of the SnTe QDs were responsible for the behavior reported a number of tests were completed using the same ligand exchange and optical tests. Blank devices demonstrated no response. HgTe QD films treated with the same ligand,[2,3] behaved in a conventional photoconductive manner. Pure SnO_2 nanoparticles in aggregated powder form demonstrated similar conductivity to the SnTe QDs but showed no response to visible or IR light. Finally spin coated SnO_2 dispersed in THF had a resistance greater than 1 GΩ and no photoresponse to visible or IR light.

Non IR illumination was provided by a Thorlabs 670 nm laser diode, any change in current upon illumination was less than the signal noise of the device. Current vs time measurements were taken with an effective sampling rate of 15 ms and a constantly applied bias. Temperature dependent conductivity measurements were taken with the same setup and filling the sample chamber with liquid nitrogen vapour to the required temperature.

SEM images were taken on a JEOL 6500 SEM, before imaging the device was carbon coated to reduce charging.

X-Ray diffraction patterns were recorded by a Panalytical X-Ray diffractometer using Cu-Kα radiation, with an operating voltage of 45 kV and current of 40 mA. The reference PDFs used were PbO_2 00-041-1492, SnO_2 00-041-1445, SnTe 00-046-1210, PbTe 00-038-1435, $Pb_{0.45}Sn_{0.55}Te$ 04-002-7237, $Pb_{0.1}Sn_{0.9}Te$ 04-018-1386.

ICP-MS samples were prepared by dissolving a solution of QDs in toluene after 4 washes, in 1 ml nitric acid. This was then diluted by a factor of 10^5 before measurement.

| Sample	OLA 80 % (ml)	ODE (ml)	Sn (mmol)	Te (mmol)	Pb (mmol)
9 nm SnTe	2.5	17.5	0.4	0.4	-
10 nm SnTe	5	15	0.4	0.4	-
12 nm SnTe	12.5	7.5	0.4	0.1	-
14 nm SnTe	15	5	0.4	0.4	-
PbSnTe	12.5	7.5	0.4	0.73	0.1
Te NW soln	1	19	0.4	0.4	-

Table S3. Details of materials used for the preparation of the QDs used in the data.

The use of reduced Te in the preparation of the 12 nm particles was reproduced in other samples to see if it was responsible for the increased responsivity however the behavior did not transfer to the other sized particles.

## SJ. PbSnTe synthesis reliability and feature position

The synthesis method detailed above reliably produces Pb doped SnTe but with varying ratios of Pb. The repeatability with regard to composition is not particularly good for this synthesis and for this reason samples with ideal ratios for device preparation had to be selected from a larger number of samples. PbSnTe devices were made from QDs that most closely matched the previously reported stoichiometry of $Pb_{0.3}Sn_{0.7}Te$, which is considered ideal for MIR sensing.[1]

The figure below shows the drop cast ATR films of three batches that were made with identical chemicals under identical conditions.
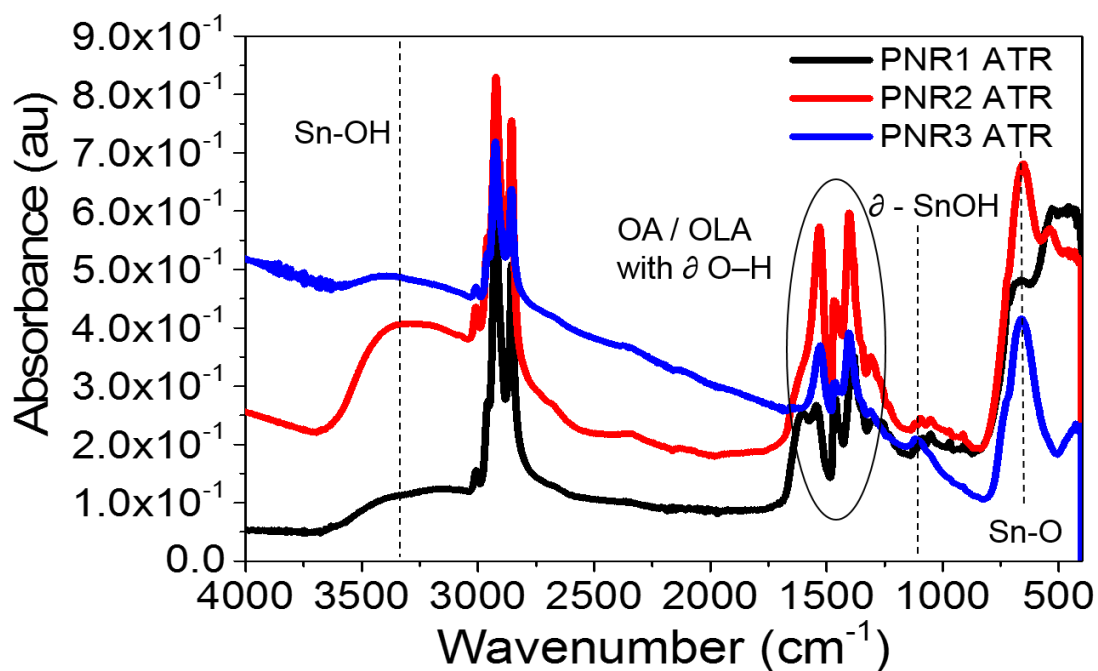
Figure S16. PbSnTe preparation variability. Each of the spectra above were prepared under identical conditions. These show a large variation in apparent bandgap and Sn-OH/Sn-O feature size. Data is not normalized.

The fact that the Sn-OH feature does not move at all between these syntheses adds weight to the argument that it is a chemical signal rather than a band (intra- or inter-band) absorption or LSPR. Five separate PbSnTe batches are shown below.
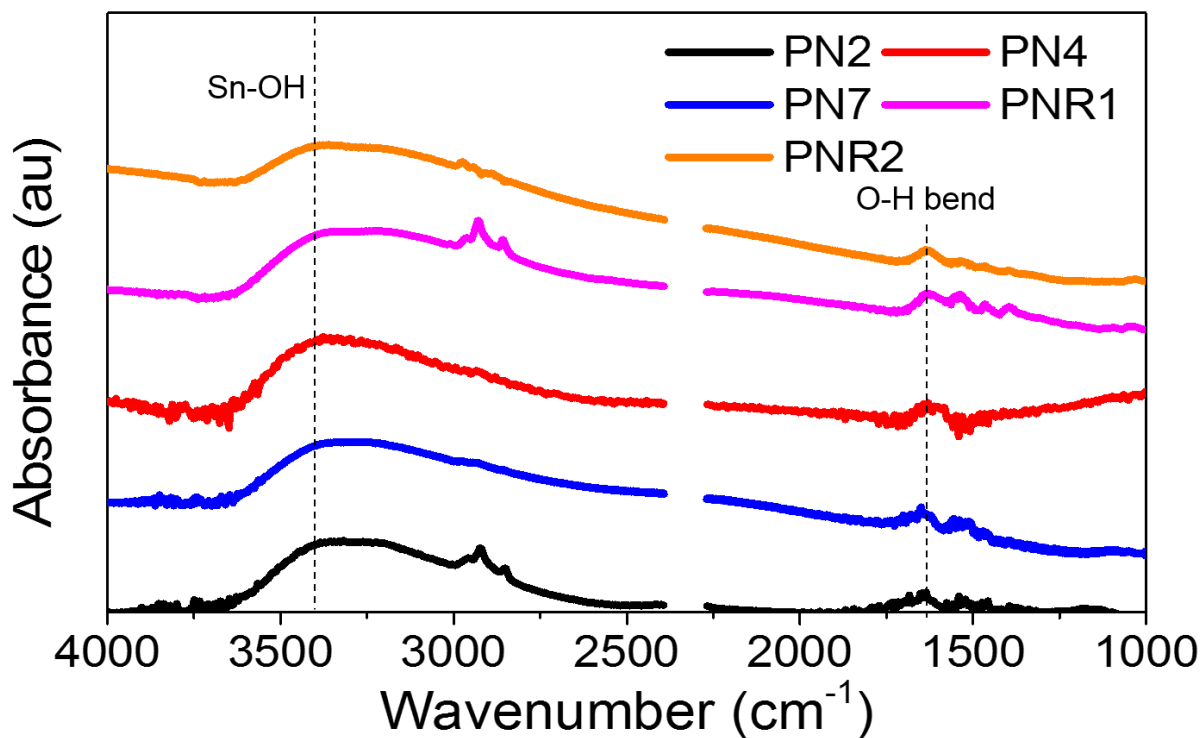
Figure S17. Film absorbance for various PbSnTe samples. The feature position is always in the same place. Regardless of any other QD or film parameter. Here the absorbance spectra have been normalized at the Sn-OH peak position and y-separated.

(1) Arachchige, I. U.; Kanatzidis, M. G. Anomalous Band Gap Evolution from Band Inversion in $Pb_{1-x}Sn_xTe$ Nanocrystals. *Nano Lett.* **2009**, *9*, 1583–1587.

(2) Bonu, V.; Das, A.; Amirthapandian, S.; Dhara, S.; Kumar Tyagi, A. Photoluminescence of Oxygen Vacancies and Hydroxyl Group Surface Functionalized SnO_2 Nanoparticles. *Phys. Chem. Chem. Phys.* **2015**, *17*, 9794–9801.

(3) Shaalan, N. M.; Hamad, D.; Abdel-Latief, A. Y.; Abdel-Rahim, M. A. Preparation of Quantum Size of Tin Oxide: Structural and Physical Characterization. *Prog. Nat. Sci. Mater. Int.* **2016**, *26*, 145–151.

(4) Seema, H.; Kemp, K. C.; Chandra, V.; Kim, K. S. Graphene–SnO_2 Composites for Highly Efficient Photocatalytic Degradation of Methylene Blue under Sunlight. *Nanotechnology* **2012**, *23*, 355705.